High-Performance Capacitors Based on MoS₂ Nanosheets Supported on Carbon Fibers

Xiaojun Liu[1], Ke Liu[2], Weijia Zhou[1,*], Ligui Li[1], Kai Zhou[1], and Shaowei Chen[1,2,*]

[1]*New Energy Research Institute, School of Environment and Energy, South China University of Technology, Guangzhou Higher Education Mega Center, Guangzhou, Guangdong 510006, China*
[2]*Department of Chemistry and Biochemistry, University of California, Santa Cruz, California 95064, United States*

ABSTRACT

MoS₂ nanosheets are grown on the surface of carbon fibers by a facile one-step hydrothermal method, forming a core–shell nanocomposite, as manifested in scanning/transmission electron microscopy, Raman scattering, and X-ray diffraction measurements. Electrochemical studies show that the core–shell nanocomposites exhibit enhanced capacitance performance in comparison with MoS₂ nanoparticles or bare carbon fibers alone, with a specific capacitance as high as 474.4 F/g at the current density of 1 A/g in 1 M Na₂SO₄ aqueous electrolyte and excellent long-term cycle stability with only 3.1% loss of the capacitance after 3,000 charge/discharge cycles. This is accounted for by the large effective surface area of the MoS₂ nanosheets as well as good electronic conductivity of the nanocomposites.

KEYWORDS: MoS₂ Nanosheet, Carbon Fiber, Core–Shell Nanocomposite, Hydrothermal, Supercapacitor.

ARTICLE

1. INTRODUCTION

As a unique energy storage device, supercapacitors have attracted increasing attention in recent years, because of their fast charge and discharge dynamics, high power performance, long cycle life, and relatively low costs.[1–4] Thus, supercapacitors have been used widely in diverse areas such as hybrid electrical vehicles, digital telecommunication, computer systems, etc. In general, there are two types of supercapacitors based on the energy storage mechanisms: electrical double-layer capacitors (EDLC) which store energy based on ion adsorption and pseudocapacitors that rely on fast surface redox reactions.[5–7] Of these, various carbon materials including carbide-derived carbon, activated carbon,[8] carbon nanotubes,[9–11] graphene sheets,[12–14] and carbon fibers (CFs) have been used extensively as electrode materials. Among these, CFs represent one of the most attractive materials, benefiting from their high mechanical flexibility, electrical conductivity, large surface area and excellent chemical stability in a wide variety of electrolytes. In a recent study, we demonstrated that conventional CFs might be used to prepare porous core–shell carbon electrodes for the fabrication of high-performance all-carbon supercapacitors.[15] Notably, CFs can also serve as a unique structural scaffold to support active materials such as MoS₂ and MnO₂ in the preparation

of small-size, lightweight and flexible supercapacitors with much enhanced capacitance performance.[16, 17]

Among these, two–dimensional (2D) nanosheet materials such as MoS₂, VS₂, SnS₂, CoS₂ and WS₂[5, 14] have been attracting particular attention. For instance, MoS₂ features a two-dimensional layered structure that is similar to that of graphene, the Mo atomic layer is sandwiched between two sulfur layers via covalent bonding, and the MoS₂ layers are stacked by van der Waals interactions, which facilitate reversible intercalation/extraction of foreign ions, such as Li⁺, Na⁺, and H⁺.[18] In addition, the Mo atoms in the center possess a range of oxidation states from +2 to +6, where the pseudocapacitance contributions may drastically enhance the overall capacitance performance that is anticipated to be comparable to that of RuO₂ and MnO₂, with a theoretical specific capacitance up to ~1000 F/g.[2, 19, 20] In fact, MoS₂ has been used extensively in lithium ion batteries,[21, 22] catalysts,[23] and phototransistors[24] due to their unique morphology, excellent mechanical and electrical properties. More recently, considerable efforts have been devoted to the preparation of MoS₂ nanostructures as the competitive electrode materials for supercapacitor applications. For instance, Soon et al.[18] prepared highly edge-oriented MoS₂ films by a thermal evaporation method which exhibited a maximum specific capacitance of 100 F/g at a potential scan rate of 1 mV/s. Cao et al.[19] prepared two-dimensional MoS₂ films-based microsupercapacitors by simple and low-cost spray painting of MoS₂ nanosheets on Si/SiO₂ chips followed by laser patterning, which featured a high area

capacitance of 8 mF/cm^2 and volumetric capacitance of 178 F/cm^3 in aqueous electrolytes.

It should be noted that the capacitance performance of MoS$_2$ depends strongly on the morphology and dimensions, and the reversible capacity may be further improved by loading MoS$_2$ nanoparticles/nanosheets on carboneous supports forming a hierarchical architecture.[25, 26] For instance, Hu et al.[27] synthesized porous tubular C/MoS$_2$ nanocomposites using porous anodic aluminum oxide as a template. The nanocomposites delivered a high capacitance of 210 F/g at 1 A/g and exhibited excellent long-term cycling stability. Huang et al.[28] prepared a hybrid material with graphene coated with layered MoS$_2$, and electrochemical measurements revealed that the maximum specific capacitance of the MoS$_2$-graphene electrodes reached up to 243 F/g at a discharge current density of 1 A/g in 1 M Na$_2$SO$_4$, Recently, Huang et al.[29] also reported a simple strategy to prepare novel 2-dimensional graphene analog MoS$_2$/MWCNT (molybdenum disulfide/multi-walled carbon nanotube) composites as supercapacitor electrode materials. The composites showed a high specific capacitance of 452.7 F/g at a current density of 1 A/g. This is the primary motivation of the present study.

Herein, by taking advantage of the unique capacitance performance of MoS$_2$ nanostructures as well as the excellent electrical conductivity of carbon fibers, we describe a simple one-step hydrothermal method to synthesize functional core–shell CF@MoS$_2$ nanocomposites where MoS$_2$ nanosheets were evenly grown on the carbon fiber surfaces in an edge-on orientation. The resulting hierarchical structures were characterized by various experimental techniques including scanning/transmission electron microscopy (SEM/TEM), X-ray diffraction (XRD), and Raman spectroscopies. Electrochemical studies showed that the resulting CF@MoS$_2$ nanocomposites exhibited a remarkable specific capacitance and excellent long-term cycle stability, suggesting that they might be used as an effective electrode material for high-performance supercapacitors.

2. EXPERIMENTAL SECTION

2.1. Chemicals
Pitch carbon fibers (CFs) were purchased from Fiber Glast Development Corporation. Sodium molybdate (Na$_2$MoO$_4 \cdot$ 2H$_2$O) and thioacetamide were purchased from Sigma-Aldrich Co. All chemicals were used without further purification. Water was supplied with a Barnstead Nanopure Water Purification System (18.3 M$\Omega \cdot$ cm).

2.2. Synthesis of CF@MoS$_2$ Nanocomposites
Experimentally, CFs were cleaned by ultrasonication in a 0.1 M H$_2$SO$_4$ solution prior to the synthesis of CF@MoS$_2$. In a typical reaction, 30 mg of sodium molybdate (Na$_2$MoO$_4 \cdot$ 2H$_2$O) and 60 mg of thioacetamide were

dissolved in 30 mL of deionized water. The solution was then transferred into a 50 mL Teflon-lined stainless steel autoclave, into which was added 20 mg of CFs. The autoclave was heated in an electrical oven at 200 °C for 24 h. The as-synthesized black products were then removed, ultrasonically cleaned for several times with deionized water and ethanol, and finally dried at 60 °C for 12 h in a vacuum oven. The resulting nanocomposites were denoted as CF@MoS$_2$ (at 11.9 wt% of MoS$_2$). For comparison, pure MoS$_2$ powders were synthesized under the same conditions but in the absence of CFs. The final products were stored in a desiccator.

2.3. Characterizations
The morphology and microstructures of the samples were characterized by scanning electron microscopy (Hitachi S-4800 field-emission SEM). Transmission electron microscopic (HRTEM) images were acquired with a JEOL JEM-2100 instrument at an acceleration voltage of 200 kV. The crystalline structures were examined by X-ray diffraction analysis (XRD, Rigaku D/Max-IIIC). Raman spectra were recorded on a RENISHAW in Via instrument with an Ar laser source of 488 nm in a macroscopic configuration.

2.4. Electrochemistry
Electrochemical measurements were carried out by using a conventional three-electrode cell containing a 1 M Na$_2$SO$_4$ aqueous electrolyte. About 3 mg of the fine core–shell carbon fibers were mixed with a 5 wt% Nafion solution and coated over a copper foil of 1×0.5 cm^2 in area. Then this coated electrode was dried at 100 °C for 10 h and was used as the working electrode. A platinum wire and Ag/AgCl (in sat. KCl) were used as the counter and reference electrode, respectively. Cyclic voltammetric (CV) measurements and galvanostatic charge/discharge tests were performed with a CHI 660E electrochemical workstation. The specific capacitance (C_s, F/g) was calculated from the cyclic voltammograms by the equation, $C_s = Q/\Delta Em$, where Q is the integrated voltammetric charge and ΔE is the voltage range of the voltammetric measurements, and m is the mass of the active material (g). The specific capacitance was also calculated from the galvanostatic discharge curves according to the equation, $C = I\Delta t/\Delta Vm$, where I is the discharge current, Δt is the discharge time, ΔV is the voltage change excluding IR drop during the discharging process, and m is the mass of the active material (g). Electrochemical impedance spectroscopic (EIS) measurements were performed at the open circuit voltage within the frequency range of 100 kHz to 0.01 Hz with the CHI 660E electrochemical workstation.

3. RESULTS AND DISCUSSION
The structures of the CF@MoS$_2$ nanocomposites were first examined by SEM measurements. From Figure 1(a), one can see that bare CFs exhibited a clean and smooth
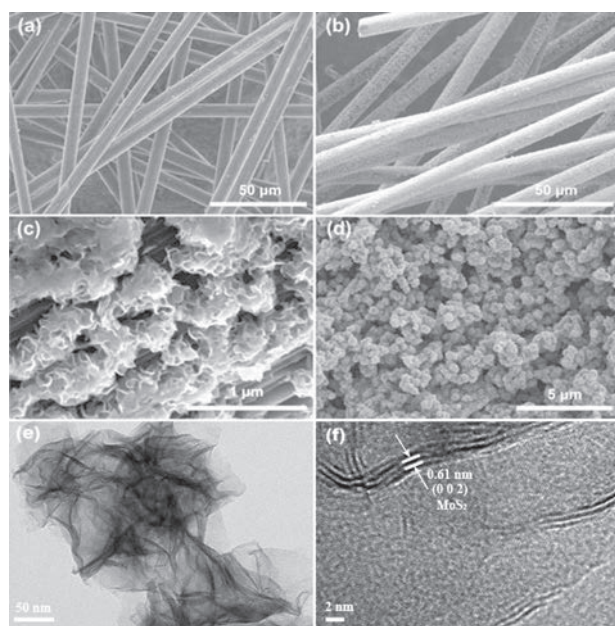
ARTICLE

Fig. 1. SEM images of CFs (a) before and (b) after the growth of MoS₂ nanosheets. Scale bars 50 μm. (c) High-magnification SEM images of MoS₂ nanosheets grown on CFs. Scale bar 1 μm. (d) SEM images of pure MoS₂ nanoparticles. Scale bar 5 μm. (e), (f) HRTEM images of MoS₂ nanosheets grown on CFs. Scale bar 50 nm and 2 nm, respectively.

surface (with a diameter of about 7 μm). In contrast, after hydrothermal reactions with sodium molybdate and thioacetamide, the surface of the CFs became apparently roughened, likely as a result of the deposition of MoS₂ nanostructures, as shown in Figure 1(b). High-magnification SEM studies in panel (c) showed that the MoS₂ nanostructures exhibited a curvy sheet-like surface morphology (up to 1 μm in length) and the MoS₂ nanosheets were grown on the CF surface largely in an edge-on orientation. This is markedly different from that of MoS₂ prepared without CFs, as depicted in panel (d), where one can see that roughly spherical MoS₂ particles (dia. about 500 nm) were formed and densely packed. Indeed, High-resolution TEM measurements of the materials scratched from the carbon fiber surface displayed an ultrathin sheet-like structure (Fig. 1(e)), with well-defined lattice fringes where the interlayer spacing of 0.61 nm is consistent with MoS₂ (002), as depicted in Figure 1(f). This is consistent with XRD results in Figure 2.

The formation of CF@MoS₂ nanocomposites was further manifested in XRD measurements. Figure 2 depicts the XRD patterns of pure MoS₂, bare CFs, and CF@MoS₂ nanocomposites. It can be seen that MoS₂ nanoparticles (blue curve) exhibited three peaks (red squares) at about 14.4°, 33.3° and 59.1°, which may be assigned to the (002), (100) and (110) crystalline planes of hexagonal MoS₂, respectively ($a = b = 0.316$ nm, $c = 1.230$ nm, JCPDS card no. 37-1492).[30, 31] For bare CFs (black curve) and CF@MoS₂ (red curve), similar patterns can be seen with a broad peak (blue circle) between 20° and 30° and
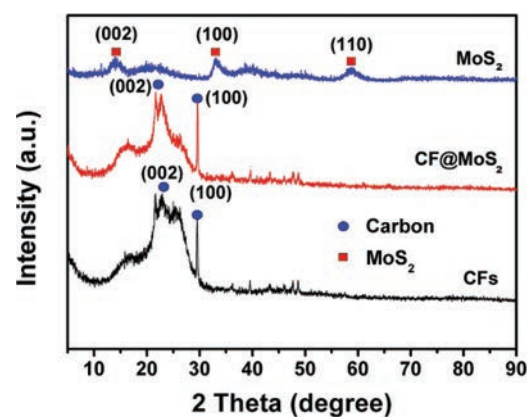
Fig. 2. XRD patterns of MoS₂ nanoparticles, CFs, and CF@MoS₂ nanocomposites.

a sharp one at 29.6° that may be respectively assigned to the graphite (002) and (100) planes. However, one may notice that the diffraction features of MoS₂ were not apparent in CF@MoS₂ nanocomposites, likely because of the low loading and/or poor crystallinity of the MoS₂ nanosheets.[32]

However, in Raman measurements (Fig. 3), it can be seen that two vibrational bands emerged at 379 cm⁻¹ (E_{2g}) and 405 cm⁻¹ (A_{1g}) with the CF@MoS₂ nanocomposites (red curve and Figure inset).[33] These are the characteristic vibrations of MoS₂, with the former due to the Mo–S stretching vibration in the basal planes of MoS₂, and the latter to the symmetric stretching vibration Mo–S of MoS₂. Furthermore, for both CFs (blue curve) and CF@MoS₂ nanocomposites, a pair of well-defined vibrational bands appeared at 1594 cm⁻¹ and 1364 cm⁻¹ which were consistent with the G and D bands of graphite (the 2D band appears as a broad peak at ca. 2750 cm⁻¹).[34–36] These further confirm the formation of CF@MoS₂ nanocomposites.
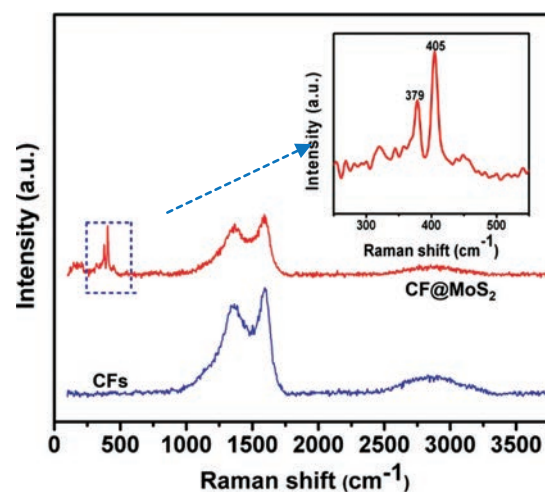
Fig. 3. Raman spectra of CFs and CF@MoS₂. Inset shows the magnification of the dashed region.

The $CF@MoS_2$ nanocomposites prepared above were then evaluated as an electrode material for supercapacitors. The performance of pure MoS_2 and bare CFs were also tested for comparison. It can be seen from Figure 4(a) that the $CF@MoS_2$ nanocomposites (red curve) exhibited an approximately square-shape cyclic voltammogram (at 50 mV/s). Consistent behaviors can be seen with MoS_2 nanoparticles (blue curve) and bare CFs (green curve) as well. Yet the significantly greater voltammetric currents of the $CF@MoS_2$ nanocomposites indicate a markedly

higher specific capacitance than the other two, most probably because of a larger electrochemical surface area and synergistic effects between MoS_2 and CFs.[37] In fact, based on the voltammetric data, the specific capacitance of CFs, MoS_2 nanoparticles and $CF@MoS_2$ nanocomposites can be estimated to be 0.4, 149.3, 503.7 F/g, respectively. The symmetric shape and the instant response upon the reversal of the electrode potential indicated that charging and discharging were highly reversible and facile. Figure 4(b) depicts the charging–discharging curves for
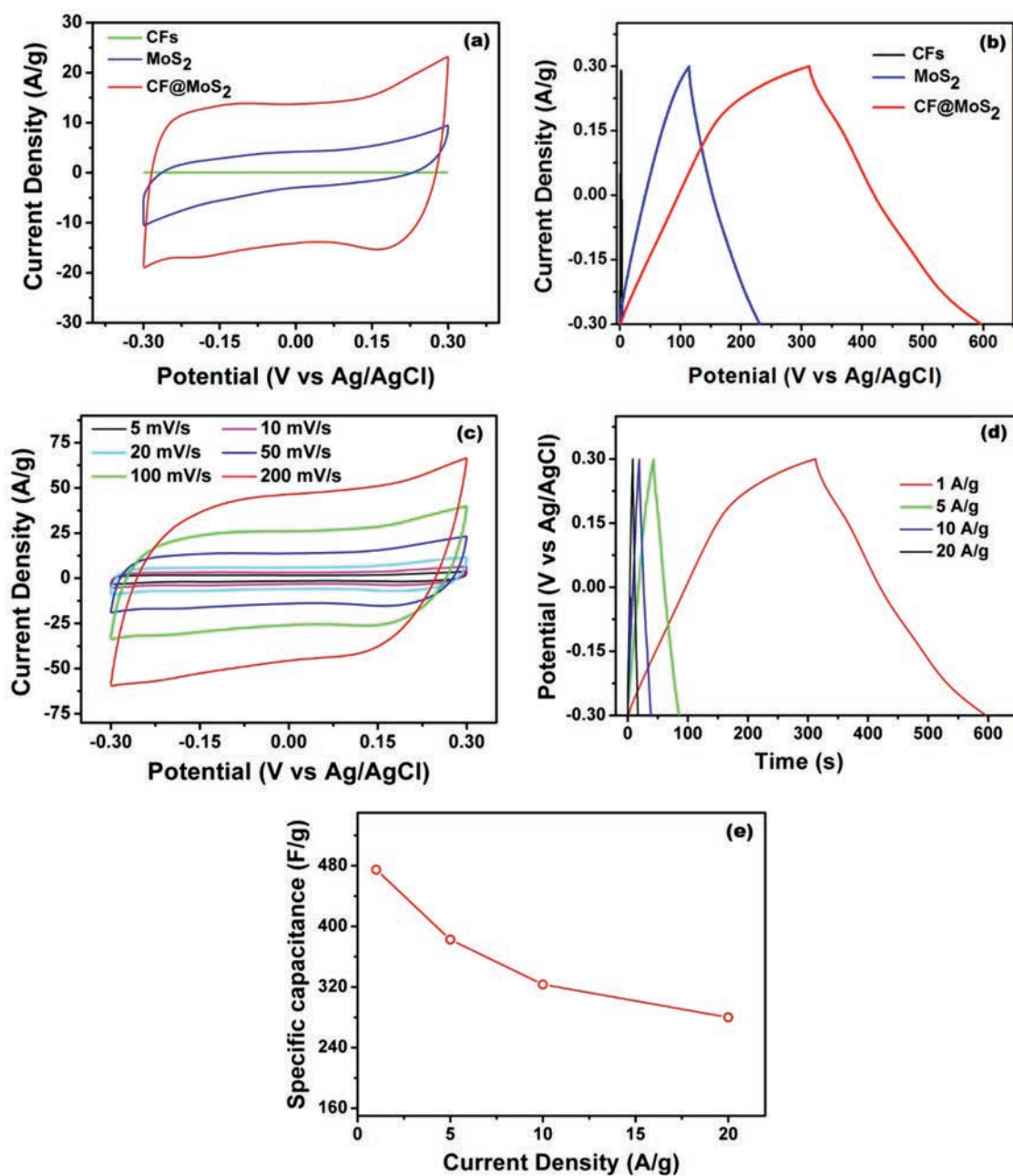
Fig. 4. (a) CV curves for bare CFs, pure MoS_2 nanoparticles and $CF@MoS_2$ at the potential scan rate of 50 mV/s. (b) Galvanostatic charging–discharging curves for the bare CFs, pure MoS_2 nanoparticles, and $CF@MoS_2$ at a current density of 1 A/g. (c) CVs for the $CF@MoS_2$ electrode at different potential scan rates, (d) Galvanostatic charging–discharging curves for the $CF@MoS_2$ electrode at different current densities, and (e) specific capacitance as a function of discharge current density.

the bare CFs, pure MoS_2 nanoparticles, and $CF@MoS_2$ at a current density of 1 A/g, where the corresponding specific capacitance was estimated to be 0.2, 114.1, and 474.7 F/g, respectively, in good agreement with the values derived from the CV curves. As shown in Figure 4(c), similar rectangular-shaped CVs were observed at other scan rates of 5, 10, 20, 50, 100 and 200 mV/s. These results indicated ideal capacitive behaviors of the $CF@MoS_2$ nanocomposites, which was further manifested in galvanostatic charging–discharging measurements at different current density with nearly symmetrical profiles, as depicted in Figure 4(d). The specific capacitance was then derived from the charging–discharging curves (Fig. 4(e)), and the values were 474.7, 382.5, 323.3 and 280.0 F/g at 1, 5, 10, and 20 A/g, respectively (note that for $CF@MoS_2$ nanocomposites at other MoS_2 loadings the capacitances were markedly lower, not shown). These are considerably higher than those reported in the literature for MoS_2-based electrodes, such as mesoporous MoS_2 synthesized by Ramadoss et al.[38] (376 and 403 F/g at a scan rate of 1 mV/s in 1 M Na_2SO_4 and KCl electrolyte solutions respectively), and porous tubular C/MoS_2 nanocomposites by Hu et al. (210 F/g at 1 A/g).[27]

Further studies were carried out by electrochemical impedance spectroscopic (EIS) measurements. Figure 5(a) depicts the Nyquist plots of the three electrodes within the frequency range of 100 kHz to 0.01 Hz at the open circuit potential with an AC perturbation of 5 mV. From the low frequency data, the capacitance (C) can be calculated using the equation $C = 1/(2\pi f Z'')$, where Z'' is the imaginary part of the impedance and f is the frequency. For the $CF@MoS_2$ electrode (red circles), the specific capacitance was estimated to be 435.8 F/g at the frequency of 0.01 Hz, in agreement with the result from the galvanostatic discharge measurements (Fig. 4). In contrast, the capacitance is only 119.7 F/g for MoS_2 alone (blue circles).

In addition, the impedance spectra can be fitted by the equivalent circuit shown as the lower inset to Figure 5(a), where R_e represents the combined contributions of ionic resistance of the electrolyte, intrinsic resistance of the substrate, and contact resistance at the active material/current collector interface, C_{dl} is the electrode double-layer capacitance, R_{ct} is the charge-transfer resistance, CPE is a constant-phase element representing the diffusive resistance (Warburg impedance) of the Faradaic process, and C_L is the limit capacitance.[39, 40] As depicted by the red and blue lines, the fittings are very good for both the MoS_2 and $CF@MoS_2$ electrodes, and the fitting results are summarized in Table I. It can be seen that the $CF@MoS_2$ nanocomposite electrode exhibited a somewhat lower R_e (1.94 Ω) than the MoS_2 one (2.41 Ω), indicating enhanced electrical conductivity of the nanocomposites. In addition, the charge transfer resistance (R_{ct}) decreases drastically from 3.99 Ω for MoS_2 to 0.12 Ω for the $CF@MoS_2$ nanocomposites, as manifested in the upper inset to Figure 5(a) by the apparent shrinking of
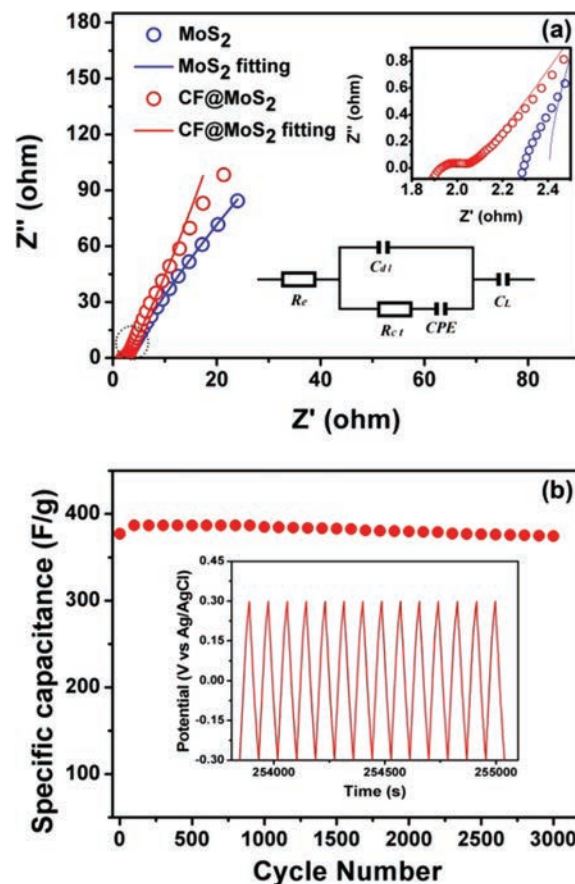
Fig. 5. (a) Nyquist plots of experimental impedance data (open circles) and fitting results (solid lines) for MoS_2 and $CF@MoS_2$ electrode at open circuit potentials in 1 M Na_2SO_4 aqueous electrolyte. Upper inset is the zoom-in of the high frequency region and the lower inset is the electrical equivalent circuit used for fitting the impedance spectra. (b) Specific capacitance versus the cycle number of the $CF@MoS_2$ nanocomposites measured at a current density of 5 A/g within an operational window of -0.3 V to $+0.3$ V. Inset is the galvanostatic charging/discharging curve after 3000 cycles.

the diameter of the semicircles in the high-frequency region. This suggests enhanced charge/discharge dynamics and hence good rate capability for the supercapacitors, as observed above in Figure 4. Meanwhile, the double-layer capacitance (C_{dl}) and the low-frequency limit capacitance (C_L) both increase by about 20 times from 33 μF to 0.62 mF and from 8.9 mF to 0.20 F, respectively. This may be accounted for by the significantly larger surface area of the $CF@MoS_2$ nanocomposites.

Table I. Fitting values of R_e, C_{dl}, R_{ct}, CPE and C_L for the experimental impedance spectra based upon the proposed equivalent circuit in Figure 5(a).

Sample	R_e (Ω)	C_{dl} (F)	R_{CT} (Ω)	CPE-T (F cm^{-2} s^{n-1})	CPE-P (n)	C_L (F)
MoS_2	2.41	3.30×10^{-5}	3.99	1.75×10^{-4}	0.71	8.87×10^{-3}
$CF@MoS_2$	1.94	6.18×10^{-4}	0.12	0.17	0.65	0.20

Because a long cycle life is also an important criterion for high-performance supercapacitors, an endurance test was conducted by galvanostatic charging/discharging cycles at 5 A/g (Fig. 5(b)). Interestingly, in the first 100 cycles the specific capacitance of the CF@MoS$_2$ nanocomposite electrode actually increased gradually and reached a maximum of 386.6 F/g. This might be attributed to an activation process due to improved contact at the electrode/electrolyte interface. The specific capacitance then decreases only slightly to 374.5 F/g after 3,000 cycles, corresponding to only 3.1% loss of the capacitance. This cycling performance of the CF@MoS$_2$ nanocomposites was markedly better than that observed with other MoS$_2$ nanostructures reported in the literature. For instance, a 8% loss was observed after only 1,000 cycles with MoS$_2$ films. That is, the CF@MoS$_2$ nanocomposite electrode prepared above shows high electrochemical stability with a long cycle life at high current densities. These remarkable features might be ascribed to several factors. First, the unique two-dimensional layered structure of MoS$_2$ may facilitate reversible intercalation/extraction of foreign ions, which is beneficial to charge transfer at the nanocomposite electrode. Second, in contrast with MoS$_2$ nanoparticles that were tightly packed, the MoS$_2$ nanosheets in the CF@MoS$_2$ nanocomposites were rather homogeneously dispersed on the CF surface with a curvy sheet-like morphology, leading to a large electrode/electrolyte interface and hence electrochemical surface area. Third, the CFs are highly conductive, leading to reduced contact resistance between the electrode materials and charge collectors.[41] That is, CFs served as an excellent current collector and a strong structural backbone for conformal coating of MoS$_2$.

4. CONCLUSIONS

In summary, a hybrid structure based on MoS$_2$ nanosheets vertically grown on CF scaffolds was prepared and used as electrode materials for high-performance supercapacitors. The as-prepared nanocomposites show significantly enhanced electrochemical specific capacitances as compared to bare CFs and MoS$_2$ nanoparticles, and the specific capacitances reached 474.7 F/g in 1 M Na$_2$SO$_4$ aqueous electrolyte at a current density of 1 A/g. The remarkable performance might be accounted for by the unique structures of the CF@MoS$_2$ nanocomposites that allowed efficient electrochemical utilization of the electrode surface for charge storage with rapid transport of ions and electrons. The nanocomposites also demonstrated excellent cycling stabilities at high current densities.

References and Notes

1. B. Wang, J. Park, D. Su, C. Wang, H. Ahn, and G. Wang, *J. Mater. Chem.* 22, 15750 (**2012**).
2. Y. Zhang, C. Sun, P. Lu, K. Li, S. Song, and D. Xue, *CrystEngComm.* 14, 5892 (**2012**).
3. K. Chen, Y. D. Noh, K. Li, S. Komarneni, and D. Xue, *J. Phys. Chem. C* 117, 10770 (**2013**).
4. K. Chen and D. Xue, *Colloids Interface Sci. Commun.* 1, 39 (**2014**).
5. F. Liu, S. Song, D. Xue, and H. Zhang, *Adv. Mater.* 24, 1089 (**2012**).
6. F. Liu and D. Xue, *Chem. Eur. J.* 19, 10716 (**2013**).
7. K. Chen, Y. Yang, K. Li, Z. Ma, Y. Zhou, and D. Xue, *ACS Sus. Chem. Engineer.* 2, 440 (**2013**).
8. D. Pech, M. Brunet, H. Durou, P. Huang, V. Mochalin, Y. Gogotsi, P.-L. Taberna, and P. Simon, *Nat. Nano* 5, 651 (**2010**).
9. V. L. Pushparaj, M. M. Shaijumon, A. Kumar, S. Murugesan, L. Ci, R. Vajtai, R. J. Linhardt, O. Nalamasu, and P. M. Ajayan, *Proc. Nat. Acad. Sci.* 104, 13574 (**2007**).
10. S. W. Lee, B.-S. Kim, S. Chen, Y. Shao-Horn, and P. T. Hammond, *J. Am. Chem. Soc.* 131, 671 (**2008**).
11. M. Kaempgen, C. K. Chan, J. Ma, Y. Cui, and G. Gruner, *Nano Lett.* 9, 1872 (**2009**).
12. T. Ramanathan, A. A. Abdala, S. Stankovich, D. A. Dikin, M. H. Alonso, R. D. Piner, D. H. Adamson, H. C. Schniepp, X. Chen, R. S. Ruoff, S. T. Nguyen, I. A. Aksay, R. K. Prud'Homme, and L. C. Brinson, *Nat. Nano* 3, 327 (**2008**).
13. K. Chen and D. Xue, *J. Colloid. Interface Sci.* 436, 41 (**2014**).
14. K. Chen, F. Liu, S. Song, and D. Xue, *CrystEngComm.* 16, 7771 (**2014**).
15. W. Zhou, K. Zhou, X. Liu, R. Hu, H. Liu, and S. Chen, *J. Mater. Chem. A* 2, 7250 (**2014**).
16. G. Yu, L. Hu, M. Vosgueritchian, H. Wang, X. Xie, J. R. McDonough, X. Cui, Y. Cui, and Z. Bao, *Nano Lett.* 11, 2905 (**2011**).
17. L. Hu, W. Chen, X. Xie, N. Liu, Y. Yang, H. Wu, Y. Yao, M. Pasta, H. N. Alshareef, and Y. Cui, *ACS Nano* 5, 8904 (**2011**).
18. J. M. Soon and K. P. Loh, *Electrochem. Solid-State Lett.* 10, A250 (**2007**).
19. L. Cao, S. Yang, W. Gao, Z. Liu, Y. Gong, L. Ma, G. Shi, S. Lei, Y. Zhang, S. Zhang, R. Vajtai, and P. M. Ajayan, *Small* 9, 2905 (**2013**).
20. K. Zhou, W. Zhou, X. Liu, Y. Sang, S. Ji, W. Li, J. Lu, L. Li, W. Niu, H. Liu, and S. Chen, *Nano Energy* 12, 510 (**2015**).
21. D. Kong, H. He, Q. Song, B. Wang, W. Lv, Q.-H. Yang, and L. Zhi, *Energy Environ. Sci.* 7, 3320 (**2014**).
22. T. Stephenson, Z. Li, B. Olsen, and D. Mitlin, *Energy Environ. Sci.* 7, 209 (**2014**).
23. F. Cesano, S. Bertarione, A. Piovano, G. Agostini, M. M. Rahman, E. Groppo, F. Bonino, D. Scarano, C. Lamberti, S. Bordiga, L. Montanari, L. Bonoldi, R. Millini, and A. Zecchina, *Catal Sci. Technol.* 1, 123 (**2011**).
24. J. Pu, L.-J. Li, and T. Takenobu, *Phys. Chem. Chem. Phys.* 16, 14996 (**2014**).
25. S. Ding, J. S. Chen, and X. W. Lou, *Chem. Eur. J.* 17, 13142 (**2011**).
26. K. Chang, W. Chen, L. Ma, H. Li, H. Li, F. Huang, Z. Xu, Q. Zhang, and J.-Y. Lee, *J. Mater. Chem.* 21, 6251 (**2011**).
27. B. Hu, X. Qin, A. M. Asiri, K. A. Alamry, A. O. Al-Youbi, and X. Sun, *Electrochimica Acta* 100, 24 (**2013**).
28. K.-J. Huang, L. Wang, Y.-J. Liu, Y.-M. Liu, H.-B. Wang, T. Gan, and L.-L. Wang, *Int. J. Hydrogen Energy*, 38, 14027 (**2013**).
29. K.-J. Huang, L. Wang, J.-Z. Zhang, L.-L. Wang, and Y.-P. Mo, *Energy* 67, 234 (**2014**).
30. K. Chang and W. Chen, *J. Mater. Chem.* 21, 17175 (**2011**).
31. Y. Li, H. Wang, L. Xie, Y. Liang, G. Hong, and H. Dai, *J. Am. Chem. Soc.* 133, 7296 (**2011**).
32. W. Zhou, Z. Yin, Y. Du, X. Huang, Z. Zeng, Z. Fan, H. Liu, J. Wang, and H. Zhang, *Small* 9, 140 (**2013**).

ARTICLE

33. Y. Hu, X. Li, A. Lushington, M. Cai, D. Geng, M. N. Banis, R. Li, and X. Sun, *ECS J. Solid State Sci. Technol.* 2, M3034 (**2013**).

34. C. Lee, H. Yan, L. E. Brus, T. F. Heinz, J. Hone, and S. Ryu, *ACS Nano* 4, 2695 (**2010**).

35. Z. Lei, J. Zhang, and X. S. Zhao, *J. Mater. Chem.* 22, 153 (**2012**).

36. K. Kong, L. Deng, I. Kinloch, R. Young, and S. Eichhorn, *J. Mater. Sci.* 47, 5402 (**2012**).

37. M.-K. Song, S. Cheng, H. Chen, W. Qin, K.-W. Nam, S. Xu, X.-Q. Yang, A. Bongiorno, J. Lee, J. Bai, T. A. Tyson, J. Cho, and M. Liu, *Nano Lett.* 12, 3483 (**2012**).

38. A. Ramadoss, T. Kim, G.-S. Kim, and S. J. Kim, *New J. Chem.* 38, 2379 (**2014**).

39. A. Di Fabio, A. Giorgi, M. Mastragostino, and F. Soavi, *J. Electrochem. Soc.* 148, A845 (**2001**).

40. M.-S. Wu, C.-Y. Huang, and K.-H. Lin, *J. Power Sources* 186, 557 (**2009**).

41. X. Xiao, T. Li, P. Yang, Y. Gao, H. Jin, W. Ni, W. Zhan, X. Zhang, Y. Cao, J. Zhong, L. Gong, W.-C. Yen, W. Mai, J. Chen, K. Huo, Y.-L. Chueh, Z. L. Wang, and J. Zhou, *ACS Nano* 6, 9200 (**2012**).

ARTICLE